## Modeling transport of soft particles in porous media

Shuaijun Li<sup>®</sup>, Hong-hui Yu<sup>®</sup>, and Jing Fan<sup>®†</sup>
Department of Mechanical Engineering, The City College of New York, New York, New York 10031, USA

(Received 18 February 2021; revised 30 July 2021; accepted 2 August 2021; published 30 August 2021)

Flow-driven transport of soft particles in porous media is ubiquitous in many natural and engineering processes, such as the gel treatment for enhanced oil recovery. In many of these processes, injected deformable particles block the pores and thus increase the overall pressure drop and reduce the permeability of the particle-resided region. The change of macroscopic properties (e.g., pressure drop and permeability) is an important indicator of the system performance, yet sometimes impossible to be measured. Therefore, it is desirable to correlate these macroscopic properties with the measurable or controllable properties. In this work, we study flow-driven transport of soft particles in porous media using a generalized capillary bundle model. By modeling a homogeneous porous medium as parallel capillaries along the flow direction with periodically distributed constrictions, we first build a governing differential equation for pressure. Solving this equation gives a quantitative correlation between the total pressure drop and measurable parameters, including concentration and stiffness of particles, size ratio of particle to pore throat, and flow rate. The resultant permeability reduction is also obtained. Our results show that the total pressure drop and permeability reduction are both exponentially dependent on the particle concentration and the size ratio of particles to pore throat. With no more than two fitting parameters, our model shows excellent agreements with several reported experiments. The work not only sheds light on understanding transport of soft particles in porous media but also provides important guidance for choosing the optimal parameters in the relevant industrial processes.

## DOI: 10.1103/PhysRevE.104.025112

#### I. INTRODUCTION

Flow-driven transport of soft units in porous media exists in many natural and engineering processes, such as enhanced oil recovery, dead-end filtration, and microfluidic cell sorting [1-6]. In many of these processes, injected deformable particles block the pores and thus increase the overall pressure drop of the particle-resided region. The change of macroscopic properties (e.g., pressure drop and permeability) is an important indicator of the system performance, yet sometimes impossible to be measured. For example, enhanced oil recovery (EOR) can be realized by injecting gel particles, or microgels, into the oil reservoir which improves the sweep efficiency and reduces excess water production [1,7– 11]. Specifically, injected microgels deform at pore throats as they flow through the medium which induces a high flow resistance locally at the pores. Many such local increments of flow resistance associate with an elevated overall flow resistance in the region, or a reduction of permeability. Consequently, the following injected fluid is forced to enter adjacent regions. The efficacy of this EOR technique depends on the permeability reduction in the gel treated region, which cannot be directly measured in the oilfields.

The mechanisms of microgel transport in porous media have mostly been studied phenomenogically and qualitatively in micromodels, sandpacks, and through coreflooding. At the pore scale, microgels exhibit six patterns of propagation behaviors—direct pass, adsorption and retention, deform and pass, shrink and pass, snap-off and pass, and trap—depending on the gel size, strength, pore structure, and gel-solid interation [9]. At the macroscale, microgels can pass through the porous medium if the driving pressure gradient is above a threshold, which increases with the gel strength and the size ratio of gel to pore throat [9]. In particular, this pressure gradient threshold is shown to increase exponentially with the gel-throat diameter ratio according to some sandpack experiments [12–14]. Moreover, the overall pressure drop for a certain porous medium increases with microgel concentration and flow rate [14,15]. However, the residual resistance factor, a measure of gel injection-induced permeability reduction and defined as the ratio of pressure gradient after gel injection to that before gel injection, decreases with flow rate [8,15]. Although significant progress has been made through extensive experimental studies in capturing microgel transport behaviors in porous media, there is a lack of studies, experimental or modeling, that provide a quantitative interpretation about the dependence of permeability reduction on various measurable or controllable properties. Such properties are usually at the pore scale, including the pore throat size, the pore velocity, and the size, concentration, and mechanical properties of microgels.

Historically, capillary bundle models were developed to study the absolute permeability of granular beds, which represent realistic porous media in a variety of applications [16–18]. The model approximates a granular bed as a group of straight channels parallel to flow direction, which allows for

<sup>\*</sup>yu@ccny.cuny.edu

<sup>†</sup>jfan1@ccny.cuny.edu

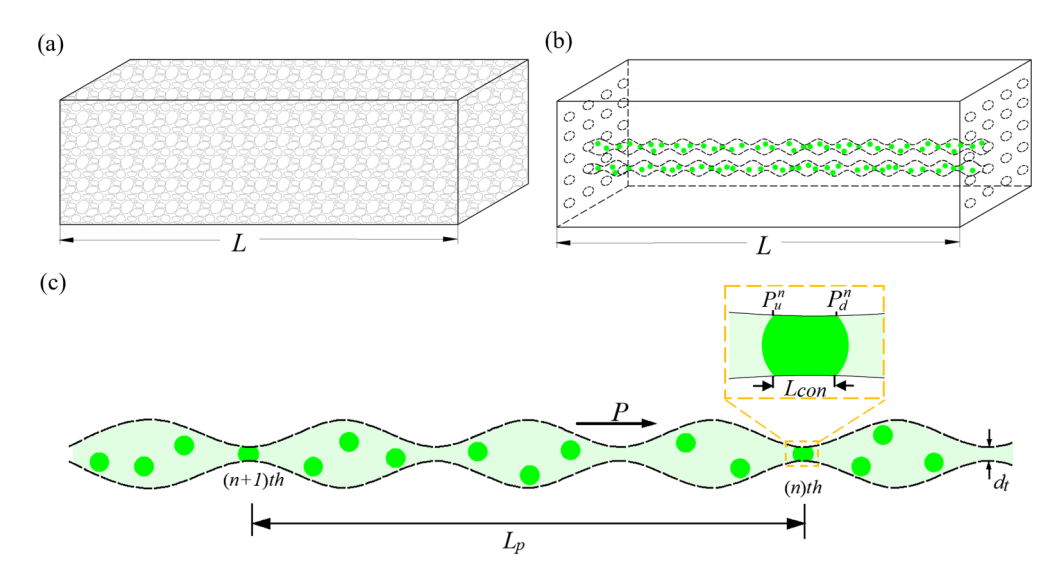


FIG. 1. Illustration of (a) homogeneous porous medium; (b) generalized capillary bundle model; (c) microgel suspension flowing in capillary.  $L_P$  is the distance between two successive deformed microgels in throats. Inset: a deformed microgel marked with the contact length and the pressures at upstream and downstream side of the microgel.

the expression of flow resistance from Hagen Poiseuille law. Further considering the analogy between Hagen Poiseuille law and Darcy's law, the permeability is correlated with microscopic structure of the porous medium [16]. In later studies on emulsion flow in porous media, capillaries with a sinusoidal structure were adopted to derive the pressure drop [19–21]. The effectiveness of the proposed capillary bundle models is then verified by comparing with experimental measurements.

In this paper, we propose a generablized capillary bundle model to quantitatively study the dependence of macroscale properties after gel injection, i.e., total pressure drop and permeability, on the measurable or controllable properties including microgel concentration and stiffness, size ratio of gel to pore throat, and Darcy flux. We consider monodisperse microgels moving with the fluid through a homogeneous porous medium with pore throats smaller than the microgels. The microgels are assumed to be uniformly distributed and pass through the pores in a similar manner without trapping, breakup, or shrinkage. The generalized capillary bundle model consists of periodic constrictions along the flow direction and retains the same porosity, permeability, pore throat size, and overall medium size as the original porous medium. We identify two sources of pressure drop due to the viscous flow and the temporary pore blockage by gels, respectively. Based on our previous study on gel blockage induced pressure drop over a constriction [22], we obtain a discrete pressure recurrence relation which leads to a differential governing equation after homogenization at the macroscale. By solving this equation, we examine the dependence of the total pressure drop and permeability reduction on other measurable properties. Finally, we compare the predictions from our model with reported experimental data.

## II. MODEL DEVELOPMENT

When microgels are flowing with the carrying fluid in a porous medium, they are either in the confined state, at which

gels are squeezed and sliding through the pore throat, or the unconfined state, at which gels are moving with fluid in the pore body. We assume that the microgel concentration is sufficiently small so that the microgels do not influence each other. Since the length scale of the porous medium is significantly larger than the pore size, the process can be regarded as the continuous motion of microgels in a group of capillaries with alternating constrictive throats and unconfining sections. We introduce a generalized capillary bundle model consisting of parallel capillaries along the flow direction with periodically distributed constrictions of a throat diameter  $d_t$ , the same as the pore throat size of the original porous medium. The constrictions are positioned randomly across the model, and thus at any cross-section perpendicular to the flow direction the ratio of total pore area to cross-sectional area is equal to porosity. We use this model to facilitate the development of a quantitative pressure correlation without specifying the shape of the constrictions. Figures 1(a) and 1(b) schematically show a homogeneous porous medium and the generalized capillary bundle model with two capillaries being illustrated. Microgels are displayed as green spheres. When passing through a constriction, the microgel deforms and induces an elevated local pressure drop,  $P_u^n - P_d^n$ , where  $P_u^n$  and  $P_d^n$  are the pressures at upstream and downstream side of the microgel. The distance between two consecutive deformed microgels is denoted as  $L_P$ , as shown in Fig. 1(c).

We consider the flow of microgel suspension in steady state. Total pressure drop results from the resistances to microgels passing-through the throats and viscous flow, which are evaluated separately. We set the cylindrical coordinates with z axis along the centerline toward the flow direction and z=0 at the inlet, and r axis the radial direction. For a microgel sliding through a confining constriction, the pressure difference across the gel balances the frictional resistance between the gel and the wall. In our previous work, we derived the governing equation for the axial normal stress inside a deformed microgel that follows the nonlinear Neo-Hookean material law for large deformation and the Amontons' friction

law considering adhesion between the gel and the channel wall [22]. Following the same methodology, we obtain the governing equation for the axial normal stress  $\sigma_z$  in a microgel with negligible adhesion:

$$\frac{d\sigma_z}{dz} + \frac{4\mu}{d_t}\sigma_z = -\frac{4\mu E}{3d_t} \left(\lambda_r^2 - \frac{1}{\lambda_x^4}\right),\tag{1}$$

where  $d_t$  is the pore throat diameter,  $\mu$  the friction coefficient, E the Young's modulus of the gel, and  $\lambda_r$  the radial stretch ratio of the gel.

Numbering the microgels that are in contact with the throats from outlet to inlet as 1, 2, 3, ... and denoting the boundary condition on the downstream side of the (n)th microgel as  $\sigma_z = -P_d^n$ , we can solve Eq. (1) and obtain  $\sigma_z$  on the upstream side,  $-P_u^n$ . We have

$$P_{u}^{n} = e^{\frac{4\mu L_{\text{con}}}{d_{t}}} P_{d}^{n} + \int_{L_{\text{con}}} \frac{4\mu E}{3d_{t}} \left(\frac{1}{\lambda_{r}^{4}} - \lambda_{r}^{2}\right) e^{\frac{4\mu}{d_{t}}z} dz, \qquad (2)$$

where  $L_{\rm con}$  is the contact length between the microgel and the capillary wall, shown in Fig. 1(c).  $e^{\frac{4\mu L_{\rm con}}{d_t}}$  can be written as  $e^{\mu f(\Psi)}$ . The dimensionless function f is a monotonic increasing polynomial function of  $\Psi$ , as derived in Appendix A. According to our previous study [22], the integral in Eq. (2) can be approximated as  $E\mu g(\Psi,\mu)$ , in which  $\Psi$  is the ratio of microgel diameter to throat diameter and g is a product of a third power polynomial of  $\Psi$  with an exponential function of  $\Psi$  (Appendix A). Thus, the relation between the upstream and downstream pressure over the (n)th microgel is  $P_u^n = e^{\mu f(\Psi)}P_d^n + E\mu g(\Psi,\mu)$ .

Denoting the viscous pressure drop between two consecutive deformed microgels as  $\Delta P_f$ , we have  $P_d^{n+1} = P_u^n + \Delta P_f$ . Therefore, pressure recurrence relation between the (n)th and (n+1)th deformed microgel is

$$P_d^{n+1} = e^{\mu f(\Psi)} P_d^n + \Delta P_f + E \mu g(\Psi, \mu). \tag{3}$$

On average,  $\Delta P_f$  is characterized by Darcy's law:  $\Delta P_f = \frac{\eta \mathcal{Q} L_p}{A\kappa}$ , where  $\eta$  is dynamic viscosity of the microgel suspension; Q is total flow rate; A is the cross-section area and  $\kappa$  is the absolute permeability of the porous medium. As derived in Appendix B,  $L_P = \frac{2\Psi^3 c\sqrt{\kappa}}{3\alpha\beta}$ , where  $\alpha$  represents microgel volume concentration, c a factor related to microstructure of the porous medium, and  $\beta$  the percentage of deformed microgels over all microgels at any instant, or the probability of a microgel being deformed by the capillary wall. Since the numerator  $2\Psi^3 c\sqrt{\kappa}$  represents a length scale comparable to the pore size and the denominator  $3\alpha\beta$  is on the order of  $10^{-2}$  or smaller (in real gel treatment processes, for example,  $\alpha$  is on the order of  $10^{-3}$ – $10^{-2}$ ), Darcy's law is applicable over the length scale of  $L_P$ .

Next we homogenize the discrete recurrence relation into a differential equation. Rewriting Eq. (3) as  $\frac{P_d^{n+1}-P_d^n}{L_p}=\frac{(e^{\mu f(\Psi)}-1)}{L_p}P_d^n+\frac{\Delta P_f+E\mu g(\Psi,\mu)}{L_p}$ , replacing the finite difference with differential form on the left side of the equation and substituting  $L_P=\frac{2\Psi^3c\sqrt{\kappa}}{3\alpha\beta}$  on the right side, we obtain the differential governing equation for pressure at the

macroscale:

$$\frac{dP}{dz} + \frac{3(e^{\mu f(\Psi)} - 1)\alpha\beta}{2\Psi^3 c\sqrt{\kappa}} P = -\frac{3\alpha\beta[\Delta P_f + E\mu g(\Psi, \mu)]}{2\Psi^3 c\sqrt{\kappa}}.$$
(4)

We may consider this equation not only as the homogenization of one channel in the flow direction, but also as an average result of all the channels, i.e. the whole porous medium. Integrating Eq. (4) by introducing an integrating factor  $e^{\frac{3(e^{\mu f(\Psi)}-1)\alpha\beta}{2\Psi^3c\sqrt{\kappa}}}$  and noticing that the gauge pressure at the outlet P(L)=0, we obtain the pressure distribution along the porous medium:

$$P(z) = \left(\frac{\eta Q}{\alpha \sqrt{\kappa} AF} + E\mu G\right) \left(e^{\frac{F\alpha}{\sqrt{\kappa}}(L-z)} - 1\right).$$
 (5a)

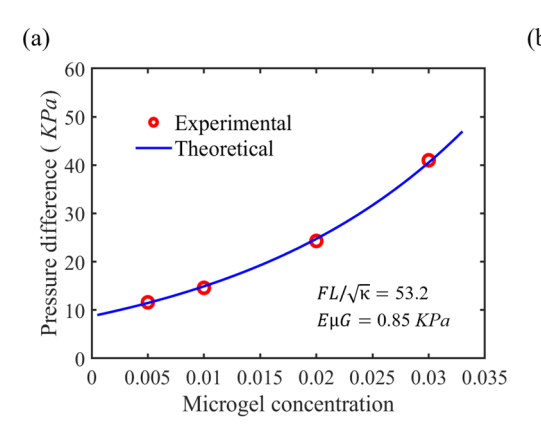
Therefore, the total pressure drop  $P_t$  over the porous medium is

$$P_{t} = \left(\frac{\eta Q}{\alpha \sqrt{\kappa} AF} + E \mu G\right) \left(e^{\frac{FL\alpha}{\sqrt{\kappa}}} - 1\right)$$
viscous flow gel deformation, (5b)

where  $F = F(\Psi, \mu) = 3\beta(\Psi)(e^{\mu f(\Psi)} - 1)/2c\Psi^3$  and  $G = G(\Psi, \mu) = g(\Psi, \mu)/(e^{\mu f(\Psi)} - 1)$  are both nondimensional. F and G characterize the mechanical interaction between the microgel and the pore throat due to size mismatch. The detailed procedure of solving Eq. (4) to obtain Eq. (5) can be found in Appendix C.

Equation (5) quantitatively correlates the total pressure drop with microgel concentration  $\alpha$ , flow rate Q, porous medium permeability  $\kappa$ , and the interaction between the microgels and the solid matrix (through F and G). The contributions from microgel deformation and viscous flow are clearly separated, as indicated in Eq. (5b). Equation (5b) reveals the exponential dependence of the total pressure drop on microgel concentration  $\alpha$  and the length of porous medium L. Moreover, since the function F depends on gel-throat size ratio  $\Psi$  exponentially, the pressure drop would be extremely sensitive to  $\Psi$ , indicating a strong on/off switching function of the medium to the gels. The effect of the gel stiffness is reflected by the term containing Young's modulus E. Besides explicitly shown next to E, the friction coefficient  $\mu$  comes into play through functions F and G. When microgel concentration  $\alpha$  is zero, which corresponds to single phase flow, Eq. (5b) recovers Darcy's law:  $P_t = \frac{\eta QL}{\kappa A}$ , by linearizing the exponential term.

Residual resistance factor  $(F_{\rm rr})$  is a major parameter used to evaluate gel treatment efficacy and defined as the ratio of injection pressure during post-gel-treatment water flooding to pretreatment water flooding.  $F_{\rm rr}$  can be calculated as  $\frac{P_t}{\eta_w} \cdot \frac{\eta_w}{\eta}$ , in which  $P_t$  and  $P_w$  are gel injection pressure [given by Eq. (5b)] and pretreatment water injection pressure, respectively;  $\eta_w$  and  $\eta$  are viscosities of water and gel suspension, respectively [12]. The ratio  $P_t/P_w$  is also referred to as the resistance factor, representing the ratio of water mobility to gel mobility. Noting that  $P_w = \frac{\eta_w QL}{\kappa A}$  based on Darcy's law,  $F_{\rm rr}$ 



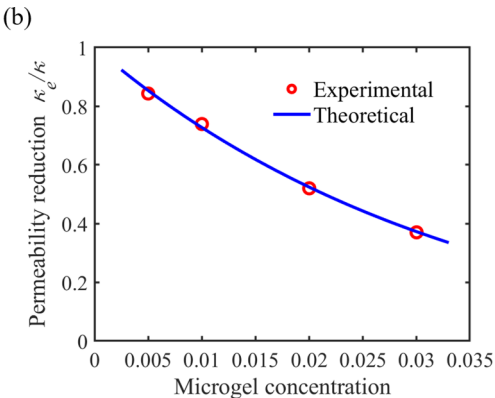


FIG. 2. Comparisons between model prediction and experimental results for the variation of (a) total pressure drop; and (b) permeability reduction with microgel concentration [14].

can be expressed as

$$F_{\rm rr} = \frac{P_t \kappa A}{\eta Q L} = \frac{\kappa}{\kappa_e}.\tag{6}$$

Here  $\kappa_e = \frac{\eta QL}{P_rA}$  is defined and regarded as the effective permeability due to microgel injection. Therefore, the ratio  $\kappa_e/\kappa$ , or the reciprocal of  $F_{\rm rr}$ , represents the permeability reduction due to gel injection.

#### III. COMPARISONS WITH EXPERIMENTS

#### A. Effect of gel concentration

Al-Ibadi and Civan [14] studied transport of microgels in porous medium experimentally with a sand column. A core sample is formed by a plastic cylinder with diameter 2.5 cm and length 18.4 cm filled with 16–20 mesh proppant sands. Permeability and porosity of the porous media were measured, which are 3.75  $\mu$ m<sup>2</sup> and 0.38, respectively [14]. Gel particle suspensions with the gel volume concentration of 0.5%, 1%, 2%, and 3% were injected into the sand-pack at a constant flow rate of 100 cm<sup>3</sup>/h. The viscosity of the suspension increases from 0.0035 Pa s to 0.0055 Pa s as the gel concentration increases over this range. For each concentration, the pressure difference was measured by a pressure transducer until the flow reached steady state, at which the measured pressure became a constant. The total pressure difference at different microgel volume concentration are plotted in Fig. 2(a) as the circles.

Based on the experimental data in Ref. [14], we fitted the parameters F and  $E\mu G$ , which are functions of friction coefficient  $\mu$ , size ratio of gel to pore throat  $\Psi$ , Young's modulus E, and porous structure of the medium. Specifically, friction coefficient  $\mu$  is included on the exponential index and thus F increases exponentially with  $\mu$ ; F also exhibits an approximately exponential trend with the size ratio  $\Psi$ . Young's modulus E only appears in the fitting parameter  $E\mu G$ . Since  $\mu$ ,  $\Psi$ , E, and the porous structure should remain the same or very similar for all the experiments in Ref. [14], F and  $E\mu G$  are two constants, and can be fitted using our model, Eq. (5b). Our model prediction agrees very well with the experimental data at  $F=5.6\times 10^{-4}$  and  $E\mu G=0.85$  KPa, which verifies the exponential dependence of pressure on

gel concentration. The comparison between the experiments and the model prediction on permeability reduction,  $\kappa_e/\kappa$  in Eq. (6), is shown in Fig. 2(b).

## B. Effect of gel size and linearization of pressure distribution

When  $\frac{FL\alpha}{\sqrt{\kappa}}$  is a small number (i.e., much smaller than 1), the pressure distribution, P(z) in Eq. (5a), is approximately a linear function of z,

$$P(z) = \left(\frac{\eta Q}{\kappa A} + \frac{E\mu H\alpha}{\sqrt{\kappa}}\right)(L - z). \tag{7}$$

Thus the residual resistance factor reduces to

$$F_{\rm rr} = 1 + \frac{E\mu H\alpha\sqrt{\kappa}A}{\eta Q},\tag{8}$$

in which H is the product of functions F and G and depends on  $\Psi$  exponentially [22]. In this case, the number of fitting parameters reduces to 1, which is  $E\mu H$ .

Wang et al. [12] investigated transport of microgels in a homogeneous sand-pack filled with unconsolidated quartz sands, which is 30 cm long with a diameter of 2.5 cm. The permeability and the porosity of the sand-pack were 6.53  $\mu$ m<sup>2</sup> and 0.32, respectively. 0.5 pore volume (PV) water followed by 3.5 PV suspension of preformed particle gels at 2 vol% were injected at the rate of 300 ml/h. The corresponding suspension viscosity is assumed to be the same value as that measured in Ref. [14] for the same microgel concentration, which is 0.0045 Pas at 2%. Four pressure taps were uniformly applied along the sand-pack to measure the pressure at different locations at steady state, as shown by the circles in Fig. 3(a). In this case,  $\frac{FL\alpha}{\sqrt{\kappa}} \sim 0.01$ . Therefore, the pressure measurements exhibited a nearly linear variation over length and can be fitted by Eq. (7) with  $E\mu H = 0.094$  KPa, as shown in Fig. 3(a). The prediction based on Darcy's law for single phase flow was also plotted as the dashed line. The striking difference clearly shows the pressure drop induced by the microgels.

Reference [12] also conducted experiments with a range of microgel size and measured the pressure gradient corresponding to each size ratio of gel to pore throat. The pressure gradients for different size ratios of gel to throat are plotted as the circles in Fig. 3(b). Since  $H(\Psi, \mu) = F(\Psi, \mu)G(\Psi, \mu)$ 

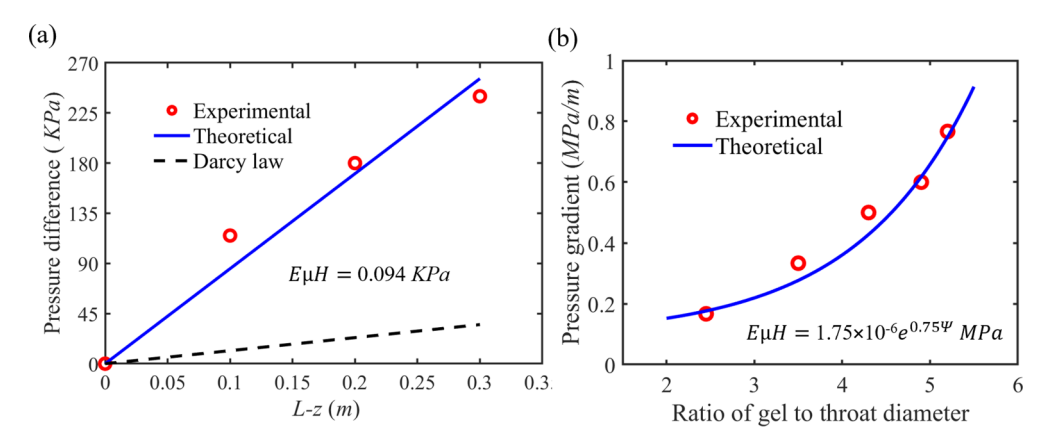


FIG. 3. Comparisons between model prediction and experimental results for the variation of (a) total pressure drop with position when  $L/\tilde{L}$  is small; and (b) pressure gradient with the ratio of gel to throat diameter [12].

increases exponentially with the size ratio  $\Psi$  [22],  $E\mu H$  in Eq. (7) can thus be approximated as  $ae^{b\Psi}$ , where a and b are two constants depending on E,  $\mu$  and the porous structure. The experimental data agree very well with our model Eq. (7) with a and b are 1.75 Pa and 0.75, respectively, as shown in Fig. 3(b). By normalizing the pressure gradient with that from Darcy's law, as plotted in Fig. 7 in Appendix D, we can clearly see the effect of microgels on increasing pressure gradient.

#### C. Effects of flow rate and friction coefficient

Saghafi *et al.* [8] studied how flow rate affects the residual resistance factor in gel particle injection. They packed crushed carbonate cores in a 51-cm-long tube with an inner radius of 3.5 mm. The permeability and porosity of the porous medium are  $135~\mu\text{m}^2$  and 0.4, respectively. Microgels with an average diameter of  $169~\mu\text{m}$  and volume concentration 0.3% were flooded through the tube with the flow rates of 0.1, 0.3, 0.5, and 0.7 ml/min. Their experiments showed that the residual resistance factor decreases with Darcy flux [ratio of flow rate to pore cross-section area,  $Q/(A\varphi)$ ], which is consistent with the prediction from our model, Eq. (6), as shown in Fig. 4(a). In the comparison, fluid viscosity  $\eta$  is estimated as water viscosity since the gel concentration is very low. Darcy flux,

 $Q/(A\varphi)$ , is the dependent variable. The experimental data can be well fitted by Eq. (6) with two fitting parameters F=0.035 and  $E\mu G=0.28$  KPa. Since  $\frac{FL\alpha}{\sqrt{\kappa}}\approx 4.57$  in this case, Eq. (8) cannot be used.

Not surprisingly, the corresponding pressure drop variation with Darcy flux also agrees well with model prediction from Eq. (5b), as shown in Fig. 4(b). Although our model predicts a linear relation between pressure and flux, we notice that the increasing rate of pressure drop from the experiments seems to decrease with the flux. This is also reflected by the sandpack experiments described in Sec. 3.1 and in Ref. [14], shown as the green crosses in Fig. 4(b). This discrepancy can be attributed to the constant friction coefficient adopted in the model. As flow rate increases, the speed of microgels passing pore throats increases. It is well studied that the friction coefficient of polymer gels is velocity dependent. The higher the speed, the lower the friction coefficient [23–26], thus resulting in a lower passing-through pressure at the throats. Therefore, the decrease of passing-through pressure compromises the linear increase of driving pressure from viscous flow and results in a falling increasing rate of total pressure drop. The current model can easily include this effect once the dependence of  $\mu$  on flow velocity is known.

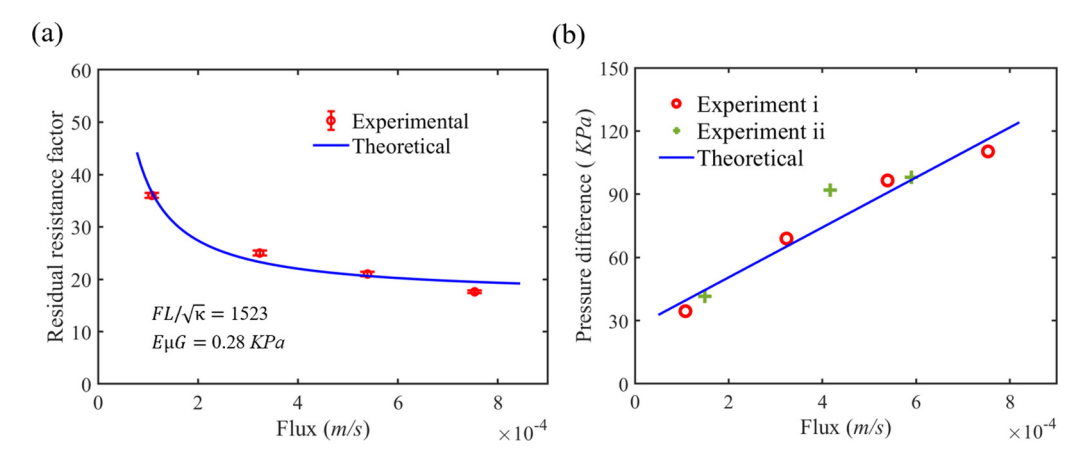


FIG. 4. Comparison between model prediction and experimental results for the variations of (a) residual resistance factor; (b) pressure drop as a function of Darcy flux. Red error bars and circles are experimental data from Ref. [8]; green crosses are experimental data from Ref. [14].

Please note that the comparable pressure drops in Refs. [8] and [14] is a coincidence. The size ratio of gel to pore throat  $\Psi$  In Ref. [8] is much larger than that in Ref. [14]; however, the gel concentration  $\alpha$  in Ref. [8] is much lower than that in Ref. [14]. Since pressure drop increases with both  $\Psi$  and  $\alpha$ , the pressure drops are comparable in these two references coincidently.

#### IV. CONCLUSION

In this work, we study how flow-driven transport of deformable particles, such as microgels, through a porous medium influences the permeability reduction, which is critical for understanding and eventually optimizing the gel treatment process for enhancing oil recovery. Since permeability can be associated with total pressure drop through Darcy's law, our work focus on building a quantitative correlation between the total pressure drop and microgel concentration, size and stiffness, flow rate, and porous medium property. We propose a generalized capillary bundle model that represents a homogeneous porous medium as parallel capillaries along the flow direction with periodically distributed constrictions mimicking the pore throats. Assuming monodisperse and uniformly distributed microgels larger than the pore throat passing through the throats in a similar manner without trapping, breakup, or shrinkage, we derive a differential governing equation with respect to the pressure in the porous medium. Solving this equation allows us to examine the dependence of the macroscopic pressure drop and permeability reduction on the measurable properties.

This analytical model, featuring sufficient simplicity and rooting from rigorous analysis, quantitatively correlates total pressure drop with flow property, microgel property, as well as porous medium property. Equation (5) clearly shows how the concentration and stiffness of microgels, size ratio of gel to pore throat, flow rate, viscosity, friction coefficient, and porous-medium's absolute permeability influence the pressure drop. The interaction between microgels and pore throats due to size mismatch are characterized by the mis-matching functions F and G, which can be determined through systematic flow experiments in the porous medium. Importantly, we find that the total pressure drop depends on microgel concentration and the length of the porous medium exponentially. Since F exponentially depends on the relative size of microgel to pore throat, the total pressure drop becomes extremely sensitive to the gel size. In addition, when the porous medium length is small compared to a characteristic length  $\tilde{L} = \frac{\sqrt{\kappa}}{F\alpha}$ , the pressure distribution exhibits a linear trend in the flow direction. Finally, when microgel concentration is zero, the model recovers Darcy's law. Our model could provide a guideline in choosing the optimal parameters in gel treatment process including gel size, concentration, and flow rate.

The generalized capillary bundle model we proposed provides a framework to study multiphase flow with dispersed particles, drops, or bubbles, through homogeneous porous media. For materials other than soft particles, certain material parameters might need to be replaced to characterize its specific characters/effects on the system. For instance, for emulsion flow through porous media, Young's modulus used for microgels should be replaced with interfacial tension. For

heterogeneous porous media, if the heterogeneity occurs at a length scale larger than that of the representative elementary volume (REV) and comparable to the system scale (scale of interest), such as stratified reservoirs, we can still apply the same methodology for the homogeneous region (on REV). Then we can conduct analysis on the system scale to evaluate the properties on the large scale, which are usually direction-dependent. If the heterogeneity occurs at a length scale larger than that of REV but smaller than the system scale, the approach depends on if the heterogeneity is spatially periodic or randomly distributed. For periodic heterogeneity, we can first use the proposed methodology to determine the macroscopic properties for each homogeneous region, then use traditional, well-developed averaging and homogenization methods at a larger scale, such as those discussed in Refs. [27,28]. In this case, the system can be regarded as homogeneous with respect to the larger-scale averaging volume. For randomly distributed heterogeneity, more complicated large-scale averaging methods would be needed; readers may refer to Refs. [29,30] for more discussions.

#### ACKNOWLEDGMENTS

Acknowledgment is made to the Donors of the American Chemical Society Petroleum Research Fund for partial support of this research (Grant No. 57496-DNI9). The work is also partially supported by NSF (Grant No. 1929502).

## APPENDIX A: EXPRESSIONS OF FUNCTION f AND g

Denote the contact length between the undeformed microgel and the capillary wall as L.  $L_{\rm con}=\int_0^L \lambda_z dZ$ . From volume conservation,  $\lambda_z=\frac{1}{\lambda_r^2}$ , where  $\lambda_r^2=\frac{(\frac{d_r}{2})^2}{R^2-(Z-\frac{L}{2})^2}$  and R is the radius of the undeformed microgel. Substituting  $\lambda_r^2$  into the integral and perform the integration, we obtain  $L_{\rm con}=\frac{2}{3}\sqrt{R^2-(\frac{d_r}{2})^2}(2\Psi^2+1)$ . Therefore,  $f(\Psi)=\frac{L_{\rm con}}{d_l}=\frac{1}{3}\sqrt{\Psi^2-1}(2\Psi^2+1)$ , which is a monotonic increasing polynomial function of  $\Psi$ .

 $E\mu g(\Psi,\mu)=\int_{L_{\rm con}} \frac{4E\mu}{3d_t}(\frac{1}{\lambda_r^4}-\lambda_r^2)e^{\frac{4\mu}{d_t}z}dz$ . This integral is identical to the second term of Eq. (6b) in Ref. [22] (noting that  $d_t=2r_0$ ); based on the experiments in constrictive channels conducted in Ref. [22], this term can be approximated as  $E\mu(\Psi^2-1)^{1.5}e^{(10.7\mu+3.6)(\Psi-1)+1}$ , as shown as the first term of Eq. (8) in Ref. [22]. Readers may refer to Ref. [22] for the details of simplification.

## APPENDIX B: SCALING OF $L_P$

To find the distance along longitudinal axis between two adjacent microgels,  $L_0$ . Assume there are  $N_1 \times N_1$  capillaries in the cross-section, shown in Fig. 5. Average distance between each capillary is  $L_c$ . Along axis, there are  $N_2$  microgels evenly distributed in each capillary. Thus, the total number of microgels in the porous medium is  $N_1^2N_2$ . The total volume that the microgels occupy is  $V_{\rm gel} = \frac{4}{3}\pi R^3N_1^2N_2$ , where R is the microgel radius. The total volume of the porous medium is  $V_{\rm total} = N_1^2L_c^2N_2L_0$ . Since  $\frac{V_{\rm gel}}{V_{\rm total}} = \frac{\alpha}{1/\varphi}$ ,  $\alpha\varphi = \frac{4\pi R^3}{3L_c^2L_0}$ . Substitute

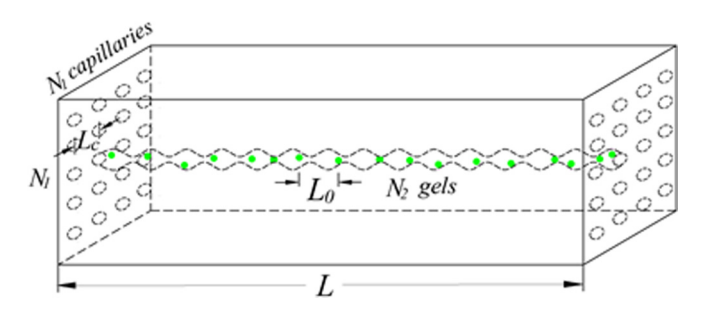


FIG. 5. Illustration of distance between two microgels in capillary:  $L_0$ .

 $\varphi=rac{rac{1}{4}\pi N_1^2 d_e^2}{N_1^2 L_c^2}$ , where  $d_e$  is the equivalent diameter of the capillary related to the microstructure of the porous medium. As a matter of fact,  $d_e$  can be correlated with macroscopic permeability  $\kappa$  by relation  $d_e = c_1 \sqrt{\kappa}$ , where  $c_1$  is a factor related to microstructure of the porous medium [31,32]. Therefore, we have  $L_0 = \frac{16R^3}{3d_e^2\alpha}$ . Since only a portion ( $\beta$ ) of microgels are confined by throats at any instant, the distance between two consecutive deformed microgels is  $L_P=\frac{L_0}{\beta}=\frac{16R^3}{3d_e^2lpha\beta}$ . Parameter  $\beta$  is the percentage of deformed microgels over all microgels at any moment, or the probability of a microgel being deformed by the capillary wall. Therefore,  $\beta$  is the ratio of the time scale that the microgel is in contact with throats to its total transport time in the porous medium. In steady state, if we assume no microgel blockage or accumulation in throats, then  $\beta$  is scaled by the ratio of the contact length  $(L_a)$  between a microgel and a throat to the distance between two neighboring throats  $L_b$ :  $L_a/L_b$  (Fig. 6).  $\beta$  may also depends on microgel material property, i.e., Young's modulus E, and friction coefficient  $\mu$ , but on a secondary level. Therefore, for a specific porous structure,  $\beta$  mainly depends on the ratio of microgel to pore throat diameter, or  $\beta = \beta(\Psi)$ . If, however, the gel completely blocks the flow, then the timescale of the blockage should be considered, which depends on the diameter ratio of the gel to the constriction, the stiffness of the gel, the friction between the gel and the channel wall, and the flow rate, which is beyond the discussion of this work. Notice that  $\Psi = 2R/d_t$ and  $d_t$  is also proportional to  $\sqrt{\kappa}$  with the proportionality depending on microstructure and porosity. For example, for random packing of spherical beads, this proportionality takes

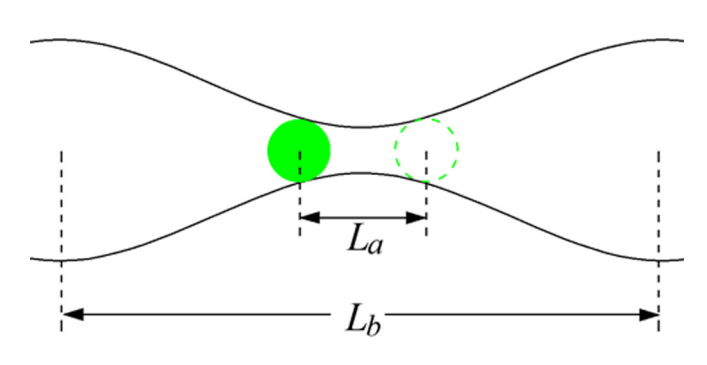


FIG. 6. Illustration of  $\beta$ : scaled by the length ratio.

the form of  $1.9\frac{(1-\varphi)\sqrt{\kappa}}{\varphi^{1.5}\Phi}$  based on the classic Kozeny-Carman equation  $\kappa=\frac{\Phi^2 d_p^2 \varphi^3}{180(1-\varphi)^2}$ , where  $\Phi$  is sphericity and  $d_p$  is grain diameter that is about  $7d_t$  [12,16,33,34]. Therefore, we have  $L_P=\frac{2\Psi^3 c\sqrt{\kappa}}{3\alpha\beta}$ , where c depends on microstructure and porosity of the porous medium.

# APPENDIX C: SOLVING PROCEDURE FROM EQS. (4) AND (5)

From Eq. (4),

$$\frac{dP}{dz} + \frac{3(e^{\mu f(\Psi)} - 1)\alpha\beta}{2\Psi^3 c\sqrt{\kappa}} P = -\frac{3\alpha\beta[\Delta P_f + E\mu g(\Psi, \mu)]}{2\Psi^3 c\sqrt{\kappa}}.$$

Solve the above equation by introducing an integrating factor  $e^{\frac{3(e^{\mu f(\Psi)}-1)\alpha\beta}{2\Psi^3c\sqrt{\kappa}}}$ ,

$$\begin{split} P(z) &= e^{-\frac{3(e^{\mu f(\Psi)}-1)\alpha\beta}{2\Psi^3c\sqrt{\kappa}}z} \bigg(\int_0^z \frac{-3\alpha\beta[\Delta P_f + E\mu g(\Psi,\mu)]}{2\Psi^3c\sqrt{\kappa}} \\ &\times e^{\frac{3[e^{\mu f(\Psi)}-1]\alpha\beta}{2\Psi^3c\sqrt{\kappa}}z} dz + C\bigg), \end{split}$$

where *C* is a constant of integration.

Notice that at inlet,  $P(z = 0) = P_t$ , so  $P_t = C$ . Integrate the above equation,

$$P(z) = e^{-\frac{3(e^{\mu f(\Psi)} - 1)\alpha\beta}{2\Psi^3 c\sqrt{\kappa}} z} \left(\frac{-[\Delta P_f + E\mu g(\Psi, \mu)]}{(e^{\mu f(\Psi)} - 1)} \times \left(e^{\frac{3(e^{\mu f(\Psi)} - 1)\alpha\beta}{2\Psi^3 c\sqrt{\kappa}} z} - 1\right) + P_t\right).$$

Rearrange,

$$\begin{split} P(z) &= P_t e^{-\frac{3(e^{\mu f(\Psi)} - 1)\alpha\beta}{2\Psi^3 c \sqrt{\kappa}} z} \\ &- \frac{[\Delta P_f + E \mu g(\Psi, \mu)]}{(e^{\mu f(\Psi)} - 1)} \Big( 1 - e^{-\frac{3(e^{\mu f(\Psi)} - 1)\alpha\beta}{2\Psi^3 c \sqrt{\kappa}} z} \Big). \end{split}$$

Apply boundary condition P(z = L) = 0, we have:

$$P_t = \frac{\Delta P_f + E \mu g(\Psi, \mu)}{e^{\mu f(\Psi)} - 1} \left( e^{\frac{3(e^{\mu f(\Psi)} - 1)L}{2\Psi^3 c\sqrt{\kappa}} \alpha \beta} - 1 \right).$$

Thus, the pressure solution is

$$P(z) = \frac{\Delta P_f + E \mu g(\Psi, \mu)}{e^{\mu f(\Psi)} - 1} \left( e^{\frac{3(e^{\mu f(\Psi)} - 1)(L - z)}{2\Psi^3 c \sqrt{\kappa}} \alpha \beta} - 1 \right).$$

Notice that  $\Delta P_f = \frac{\eta \mathcal{Q} L_p}{A\kappa}$ . Substitute  $L_p = \frac{2\Psi^3 c \sqrt{\kappa}}{3\alpha\beta}$  into  $\Delta P_f$ ,  $\Delta P_f = \frac{2c\Psi^3\eta\mathcal{Q}}{3\alpha\beta A\sqrt{\kappa}}$ . Rearranging, we have

$$P(z) = \left(\frac{\eta Q}{\alpha \sqrt{\kappa} AF} + E \mu G\right) \left(e^{\frac{F\alpha}{\sqrt{\kappa}}(L-z)} - 1\right),\,$$

and at the inlet z = 0, the total pressure is

$$P_t = \left(\frac{\eta Q}{\alpha \sqrt{\kappa} AF} + E \mu G\right) \left(e^{\frac{FL}{\sqrt{\kappa}}\alpha} - 1\right),\,$$

where  $F(\Psi, \mu) = 3\beta (e^{\mu f(\Psi)} - 1)/2c\Psi^3$  and  $G(\Psi, \mu) = g(\Psi, \mu)/(e^{\mu f(\Psi)} - 1)$ . The above two equations recover Eqs. (5a) and (5b).

## APPENDIX D: NORMALIZED PRESSURE GRADIENT IN FIG. 3(b)

We normalized the pressure gradient in Fig. 3(b) by the pressure gradient from Darcy's law, as shown in Fig. 7.

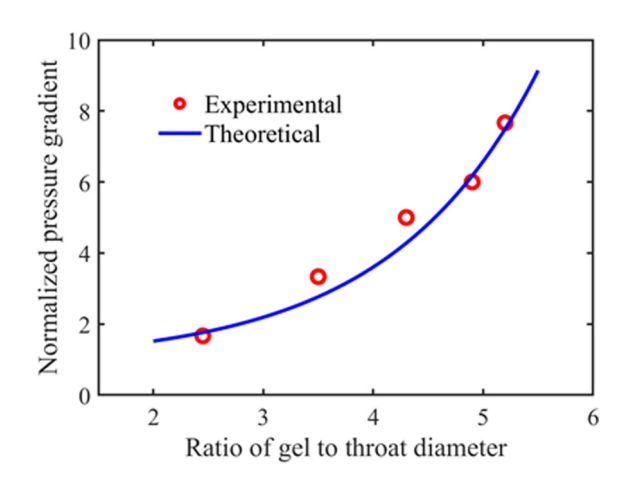


FIG. 7. Comparisons between model prediction and experimental results in Ref. [12] for the variation of normalized pressure gradient by Darcy's law with the ratio of gel to throat diameter.

- [1] B. Bai, L. Li, Y. Liu, H. Liu, Z. Wang, and C. You, Preformed particle gel for conformance control: Factors affecting its properties and applications, SPE. Reserv. Eval. Eng. **10**, 415 (2007).
- [2] N. Lebleu, C. Roques, A. Pierre, and C. Christel, Role of the cell-wall structure in the retention of bacteria by microfiltration membranes, J. Membr. Sci. 326, 178 (2009).
- [3] M. Chabert and J. Viovy, Microfluidic high-throughput encapsulation and hydrodynamic self-sorting of single cells, Proc. Natl. Acad. Sci. USA 105, 3191 (2008).
- [4] A. Z. Zinchenko and R. H. Davis, Emulsion flow through a packed bed with multiple drop breakup, J. Fluid Mech. 725, 611 (2013).
- [5] A. Z. Zinchenko and R. H. Davis, Squeezing of a periodic emulsion through a cubic lattice of spheres, Phys. Fluids 20, 040803 (2008).
- [6] M. I. Romero, M. S. Carvalho, and V. Alvarado, Experiments and network model of flow of oil-water emulsion in porous media, Phys. Rev. E 84, 046305 (2011).
- [7] M. Lin, G. Zhang, H. Zhao, Q. Zhao, and F. Sun, Conformation and plugging properties of crosslinked polymer microspheres for profile control, Colloids Surf. A Physicochem. Eng. Asp. 477, 49 (2015).
- [8] H. R. Saghafi, M. A. Emadi, A. Farasat, M. Arabloo, and A. Naderifar, Performance evaluation of optimized preformed particle gel (PPG) in porous media, Chem. Eng. Res. Des. 112, 175 (2016).
- [9] B. Bai, Y. Liu, J. Coste, and L. Li, Preformed particle gel for conformance control: Transport mechanism through porous media, SPE Reserv. Eval. Eng. 10, 176 (2007).
- [10] Y. Liu, B. Bai, and Y. Wang, Applied technologies and prospects of conformance control treatments in China, Oil Gas Sci. Technol. – Rev. IFP Energies nouvelles 65, 859 (2010).
- [11] J. J. Sheng, Modern Chemical Enhanced Oil Recovery: Theory and Practice (Gulf Professional Publishing, Burlington, MA, 2010), Chap. 1, pp. 1–9.
- [12] J. Wang, H. Liu, Z. Wang, and P. Hou, Experimental investigation on the filtering flow law of pre-gelled particle in porous media, Transp. Porous Media 94, 69 (2012).

- [13] J. Wang, H. Zhang, H. Liu, W. Zhao, H. Liu, C. Yao, J. Zheng, and Y. Shen, Quantification of transportation of deformable gel particles in porous media, in *Proceeding sof the SPE Annual Technical Conference and Exhibition* (San Antonio, TX, 2017).
- [14] A. Adnan and C. Faruk, Experimental study of gel particles transport through porous media, in *Proceedings of the SPE Latin America and Caribbean Petroleum Engineering Conference* (Mexico City, Mexico, 2012).
- [15] A. Goudarzi, H. Zhang, V Abdoljalil, P. Taksaudom, Y. Hu, M. Delshad, B. Bai, and K. Sepehrnoori, A laboratory and simulation study of preformed particle gels for water conformance control, Fuel 140, 502 (2015).
- [16] P. C. Carman, Fluid flow through granular beds, Chem. Eng. Res. Des. **75**, S32 (1997).
- [17] F. A. L. Dullien, Porous Media: Fluid Transport and Pore Structure (Academic Press, San Diego, CA, 2012).
- [18] K. Watanabe and M. Flury, Capillary bundle model of hydraulic conductivity for frozen soil, Water Resour. Res. 44, W12402 (2008).
- [19] S. Roy, A. Hansen, and S. Sinha, Effective rheology of twophase flow in a capillary fiber bundle model, Front. Phys. 7, 92 (2019).
- [20] D. Teeuw and F. T. Hesselink, Power-law flow and hydrodynamic behaviour of biopolymer solutions in porous media, in Proceedings of the SPE Oilfield and Geothermal Chemistry Symposium (Stanford, CA, 1980).
- [21] L. Yu, B. Ding, M. Dong, and Q. Jiang, A new model of emulsion flow in porous media for conformance control, Fuel 241, 53 (2019).
- [22] S. Li, H. Yu, T. Li, Z. Chen, W. Deng, A. Anbari, and J. Fan, Understanding transport of an elastic, spherical particle through a confining channel, Appl. Phys. Lett. **116**, 103705 (2020).
- [23] J. De Vicente, J. R. Stokes, and H. A. Spikes, Soft lubrication of model hydrocolloids, Food Hydrocoll. **20**, 483 (2006).
- [24] T. Fort, Jr., Adsorption and boundary friction on polymer surfaces, J. Phys. Chem. 66, 1136 (1962).
- [25] K. Tanaka, Kinetic friction and dynamic elastic contact behaviour of polymers, Wear 100, 243 (1984).

- [26] O. Torres, E. Andablo-Reyes, B. S. Murray, and A. Sarkar, Emulsion microgel particles as high-performance bio-lubricants, ACS Appl. Mater. Interfaces 10, 26893 (2018).
- [27] S. Whitaker, The method of volume averaging, *Theory and Applications of Transport in Porous Media*, Vol. 13 (Kluwer Academic Publishers, CA, 1999).
- [28] C. C. Mei and B. Vernescu, Homogenization Methods for Multiscale Mechanics (World Scientific Publishing, Singapore, 2010).
- [29] R. A. Greenkorn and D. P. Kessler, Dispersion in heterogeneous, nonuniform, anisotropic porous media, Ind. Eng. Chem. 61, 14 (1969).

- [30] M. Quintard and S. Whitaker, Two-phase flow in heterogeneous porous media: The method of large-scale averaging, Transp. Porous Media 3, 357 (1988).
- [31] D. A. Alvarado and S. S. Marsden, Jr., Flow of oil-in-water emulsions through tubes and porous media, Soc. Petrol. Eng. J. 19, 369 (1979).
- [32] M. Arhuoma, M. Dong, D. Yang, and R. Idem, Determination of water-in-oil emulsion viscosity in porous media, Ind. Eng. Chem. Res. 48, 7092 (2009).
- [33] P. C. Carman, *Flow of Gases through Porous Media* (Academic Press, New York, NY, 1956).
- [34] J. Kozeny, Über kapillare Leitung des Wassers im Boden, Sitzungsber. Akad. Wiss. Wien 136, 271 (1927).